TABLE 3. *Neuropsychological profiles of schizophrenia and epilepsy with and without psychotic disorder*

	Schizophrenia	Epilepsy with a psychotic disorder	Epilepsy without a psychiatric disorder	Group difference
Number of cases (male/female)	16 (9/7)	22 (17/5)	22 (14/8)	NS
Age (yr)	36.9 ± 10.4	37.2 ± 8.4	36.0 ± 9.3	NS
Education (yr)	13.6 ± 2.1	13.6 ± 2.2	13.9 ± 2.1	NS
Age at onset of epilepsy (yr)	–	11.2 ± 6.7	16.0 ± 11.9	NS
Age at onset of psychosis (yr)	24.0 ± 10.2	25.4 ± 4.1	–	NS
WAIS-R full-scale IQ	84.0 ± 18.4	75.6 ± 18.5	86.5 ± 14.4	[a]
Verbal IQ	86.3 ± 16.5	76.9 ± 17.4	86.4 ± 11.0	[a]
Performance IQ	84.5 ± 17.9	79.2 ± 19.1	89.4 ± 11.0	NS
Comprehension	7.1 ± 3.1	5.5 ± 2.7	7.1 ± 3.1	[a]
Similarity	7.6 ± 3.6	5.9 ± 4.0	7.1 ± 3.7	[a]
Digit span	8.6 ± 2.6	7.1 ± 2.5	7.5 ± 2.3	[a]
Digit symbol	7.0 ± 3.1	5.2 ± 3.5	7.5 ± 2.5	[a]
Picture arrangement	7.9 ± 2.8	6.4 ± 4.1	9.0 ± 3.1	[a]
WMS Memory quotient	90.0 ± 20.3	84.1 ± 15.7	91.7 ± 14.5	[a]
Nonrelated paired associate	4.8 ± 4.1	3.6 ± 3.5	5.6 ± 3.6	[a]
WCST category number	3.6 ± 2.2	3.5 ± 2.3	3.6 ± 2.5	NS

NS, not significant; WAIS-R, Wechsler Adult Intelligence Scale–Revised; WMS, Wechsler Memory Scale; WCST, Wisconsin Card Sorting Test.
[a] $p < 0.05$ (χ^2 test/analysis of variance).

REFERENCES

1. Matsuura M, Oana Y, Kato M, et al. A multi-center study on the prevalence of psychiatric disorders among new referrals for epilepsy in Japan. *Epilepsia* 2003;44:107–14.
2. Devinsky O. What do you do when they grow up? Approaches to seizures in developmentally delayed adults. *Epilepsia* 2002;43(suppl 3):71–9.
3. Adachi N, Matsuura M, Okubo Y, et al. Predictive variables of interictal psychosis in epilepsy. *Neurology* 2000;55:1310–4.
4. Lund J. The prevalence of psychiatric morbidity in mentally retarded adults. *Acta Psychiatr Scand* 1985;72:563–70.
5. American Psychiatric Association. *Diagnostic and statistical manual of mental disorders*. 4th ed, rev. Washington, DC: American Psychiatric Press, 1994.
6. Matsuura M, Adachi N, Oana Y, et al. A proposal for a new five-axial classification scheme for psychoses of epilepsy. *Epilepsy Behav* 2000;1:343–52.
7. Matsuura M, Adachi N, Oana Y, et al. A polydiagnostic and dimensional comparison of epileptic psychoses and schizophrenia spectrum disorders. *Schizophrenia Res* 2004;69:189–201.
8. World Health Organization. *ICD-10 guide for mental retardation*. Geneva: World Health Organization, 1996.
9. Toone BK, Garralda ME, Ron MA. The psychoses of epilepsy and the functional psychoses. *Br J Psychiatry* 1980;137:245–9.
10. Perez MM, Trimble MR, Murray NMF, et al. Epileptic psychosis: an evaluation of PSE profiles. *Br J Psychiatry* 1985;146;155–63.
11. Oyebode F, Davison K. Epileptic schizophrenia: clinical features and outcome. *Acta Psychiatr Scand* 1989;79:327–31.
12. Kanemoto K, Tsuji T, Kawasaki J. Reexamination of iterictal psychoses based on DSM IV psychosis classification and international epilepsy classification. *Epilepsia* 2001;42:98–103.
13. Kristensen O, Sindrup EH. Psychomotor epilepsy and psychosis, III: social and psychological correlates. *Acta Neurol Scand* 1979;59:1–9.
14. Umbricht D, Degreef G, Barr WB, et al. Postictal and chronic psychoses in patients with temporal lobe epilepsy. *Am J Psychiatry* 1995;152:224–31.
15. Kaufman AS. *Assessing adolescent and adult intelligence*. Boston, Mass: Allyn & Bacon, 1990.
16. Ferguson SM, Rayport M, Gardner R, et al. Similarities in mental content of psychotic state, spontaneous seizures, dreams and responses to electrical brain stimulation in patients with temporal lobe epilepsy. *Psychosom Med* 1969;31:479–98.
17. Mellers JDC, Toone BK, Lishman WA. A neuropsychological comparison of schizophrenia and schizophrenia-like psychosis of epilepsy. *Psychol Med* 2000;30:325–35.
18. Caplan R, Arbelle S, Guthrie D, et al. Formal thought disorder and psychopathology in pediatric primary generalized and complex partial epilepsy. *J Am Acad Child Adolesc Psychiatry* 1997;36:1286–94.

Current Biology, Vol. 15, 1–6, November 22, 2005, ©2005 Elsevier Ltd All rights reserved. DOI 10.1016/j.cub.2005.10.069

Separate Processing of Different Global-Motion Structures in Visual Cortex Is Revealed by fMRI

Shinichi Koyama,[1,2] Yuka Sasaki,[2]
George John Andersen,[3] Roger B.H. Tootell,[2]
Masato Matsuura,[4] and Takeo Watanabe[1,*]
[1]Department of Psychology
Boston University
64 Cummington Street
Boston, Massachusetts 02215
[2]NMR Center
Massachusetts General Hospital
Charlestown, Massachusetts 02129
[3]Department of Psychology
University of California, Riverside
Riverside, California 92521
[4]Tokyo Medical and Dental University
1-5-45 Yushima, Bunkyo-ku
Tokyo 113-8510
Japan

Summary

The visual system has the remarkable ability to extract several types of meaningful global-motion signals, such as radial motion, translation motion, and rotation, for different visual functions and actions. In the monkey brain, different groups of cells in MST respond best to different types of global motion [1, 2], whereas in lower cortical areas including MT, no such differential responses have been found. Here, we show that an area (or areas) lower than MST in the human brain [3] responds to different types of global motion. A series of human functional magnetic resonance imaging (fMRI) experiments, in which attention was controlled for, indicated that the center of radial motion activates the corresponding location in the V3A representation, whereas translation motion activates mainly in a more peripheral representation of V3A. These results suggest that in the human brain, V3A is an area that differentially responds according to the type of global motion.

Results and Discussion

Monkey single-unit recording studies have revealed that global-motion patterns such as rotation, radial motion, and translation motion [4–7] are processed distinctly in MST [1, 2, 8]. What evidence exists for motion processing in human brains? In contrast to monkey brains, the results of several studies suggest that V3A in human brains is highly motion selective [9, 10]. V3A is regarded as an earlier stage of visual processing than MST [3]. Greater activation with coherent motion (velocities in a single general direction), as compared with random motion, was found in V3A but not in V1 [11–13]. However, how human V3A responds to different types of global motion has not been addressed. In the present paper, we show that human V3A differentially responds according to the type of global motion.

To measure global-motion activity in multiple areas, we presented human subjects with displays of radial motion, translation motion, and random motion. Radial motion is an important source of information for locomotion (e.g., heading) and can be either expansion or contraction. Translation motion is a pattern whose direction is perceived as the average of signals of randomly moving dots within a certain range of directions [14–17]. In the present study, we found that in human V3A, greater activity was associated with retinotopic locations corresponding to the focus of expansion (FOE) as compared to activity to random motion, whereas regions associated with more peripheral retinotopic regions were more activated with translation motion than random motion.

To assess activation based on global-motion type, we used a standard method of comparing MR activity to a specific global-motion type with activity to random motion. The stimuli consisted of limited-lifetime dots to ensure that the activity of units sensitive to local motion was statistically the same for global-motion stimuli and random-dot stimuli. Thus, if a difference in activity is found between a global type of motion and a random-motion pattern in some area, it would be regarded as a result of response to a pattern on a global scale [11, 12, 18, 19] rather than local motion.

In order to compare activity of different motion types, we systematically controlled for two confounding factors: opponent-motion suppression and attention. Opponent-motion suppression refers to activity of cells for neighboring opponent-motion direction signals [20, 21]. Opponent-motion suppression has been found in monkey MT [20] or human MT+ [21], but not in V1 for either species. This finding could make the brain respond differently to translation motion and random motion. For example, a translation motion in which dots move within ±45° from the spatiotemporal average has no dots moving in opposite directions, whereas in a random-motion display, two dots could move in opposite directions within a neighboring region. Thus, higher MT+ activity in the presence of translation motion as compared with random motion can be attributed to the lack of opponent motion in the global flow. To control for this factor, we used a *transparent*-translation-motion display in which half of the dots moved randomly within a 45° range and the other half within the opposite 45° range (e.g., 0° to 45° and 180° to 225°). As a result, two transparent-translation motions in opposite directions were perceived (Figures 1A and 1B). For this manipulation, the probability of local dots moving in opponent directions (within a local region) for the translation-motion display was statistically higher than in the random-motion display. The presence of a high degree of opponent motion, as compared to little or no opponent motion, results in lower MR activity. Thus, higher activity for transparent-translation motion as compared to random motion would be the result of the global flow pattern and not opponent suppression.

*Correspondence: takeo@bu.edu

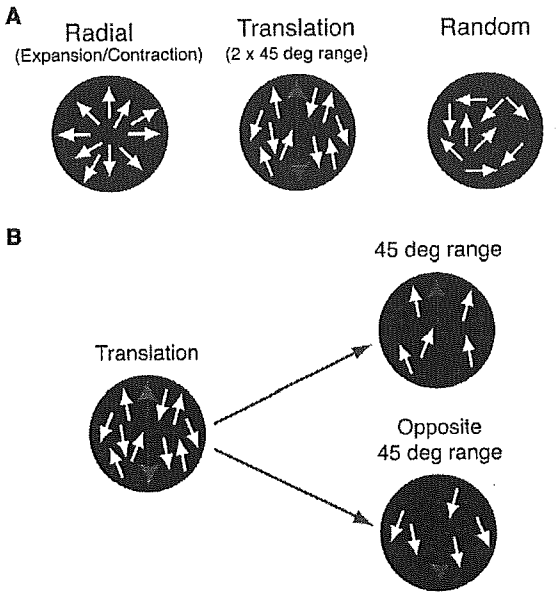

Figure 1. A Schematic Description of the Motion Stimuli

(A) The subjects viewed a radial-motion, translation-motion, or random-motion stimulus in 16 s epochs. The global-motion types were changed in a random order every 16 s.

(B) The translation-motion display consisted of two sets of global motion. In one set, the motion directions of the dots were limited to a 45° range, whereas in the other set, the motion directions of the dots were limited to the opposite 45° range. The two sets of global motion were perceived as transparent motion.

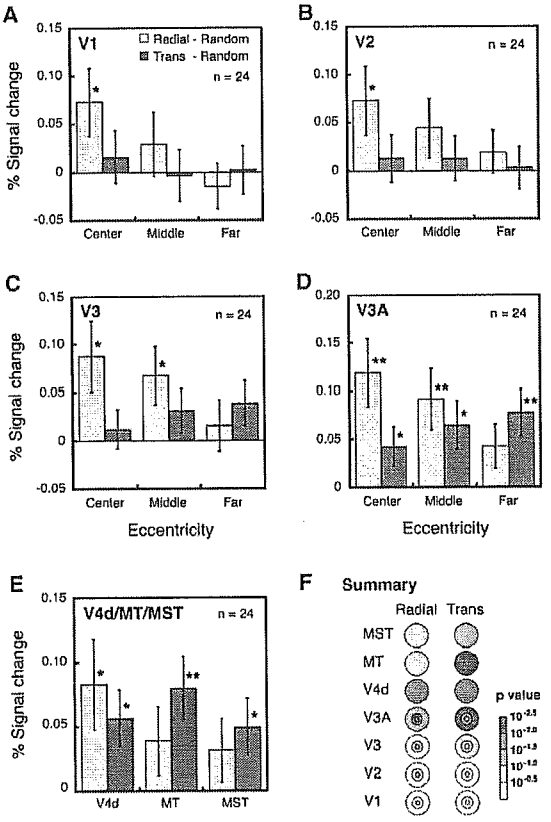

Figure 2. Mean MR Signal Amplitudes for Each Visual Area for Each Eccentricity

Each column represents the average of 24 data, i.e., 6 subjects × 4 time points. Error bars indicate the standard errors. The * sign indicates significant difference between radial motion (or translation motion) versus random motion ($p < 0.05$). The ** sign indicates $p < 0.01$. The red color scale in the summary (F) indicates p values from the paired t test for radial motion versus random motion (left column) and translation motion versus random motion (right column) for each visual area (V1, V2, V3, V3A, V4d, MT, and MST). Three concentric circles in V1, V2, V3, and V3A represent eccentricity (center < 2°, middle < 5°, and far > 5°) in those visual areas. Radial motion produced significantly stronger MR signals than random motion in the following visual areas: central V1 ($p < 0.05$), central V2 ($p = 0.052$), central and middle V3 ($p < 0.05$), central and middle V3A ($p < 0.05$), and V4d ($p < 0.05$). On the other hand, translation motion produced significantly stronger MR signals than random motion in central and middle V3A ($p < 0.05$), far V3A ($p < 0.01$), V4d ($p < 0.05$), MT ($p < 0.01$), and MST ($p < 0.05$).

As for attention, we asked subjects to perform a well-established task [22, 23] that was independent of the global-motion type. Each trial lasted for 4 s. During the first 1980 ms, a motion stimulus was presented. The subjects had to respond in the remaining 2020 ms. During the 1980 ms presentation, the speed of motion was different between the first and second intervals (both 990 ms) of a motion-stimulus presentation. Subjects were instructed to press a response key to indicate which of the two intervals had a greater speed. The same motion-speed discrimination task was given in all of the three motion types in order to ensure that subjects attended equally in all motion conditions [22, 23].

There were four trials in each epoch of 16 s. In each epoch, the same type of motion was presented: For transparent-translation motion, each of four pairs of direction ranges covering 90° in total was presented on each trial, so that 360° motion directions were covered in an epoch. For radial motion, in two trials, dots moved outward (expansion) from the center of the display, whereas in the other two trials, they moved inward (contraction). The presentation order of the four trials was randomized. For random motion, local dots moved within the 360° range for an entire epoch. The dot density was kept constant throughout the region in all the types of motion so that local-motion signals were equivalent. Within one scan, the same set of local-motion signals were presented for the three types of motion. We measured fMRI activity on a flattened occipital patch that indicated the retinotopical locations in V1, V2, V3 [24, 25], the locations of MT/MST [26], and other areas including V4d [27], V3B [28], and KO [29] as well as V3.

A larger amount of MR signal for the radial motion or translation motion, as compared to the random motion, can be regarded as activity related to the overall pattern of radial or translation motion. The activity patterns for these two types of motion were dramatically different in these low-level stages. Figures 2A–2E and Figure 3 indicate that the general tendency of activity for translation motion increased with increasing eccentricity in relatively higher stages such as V3 and V3A. On the other hand, activity for radial motion decreased with increasing eccentricity in V1, V2, V3, and V3A. A two-way ANOVA for motion type (radial versus random motion)

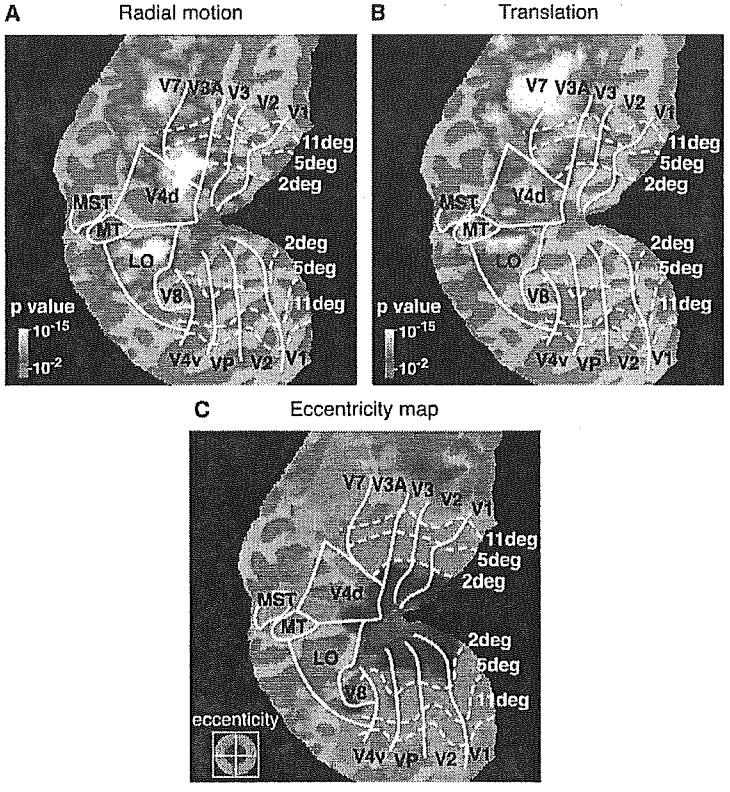

Figure 3. Activation Maps from the First Experiment

(A) Activation map for radial motion in a representative subject (left hemisphere). Average activation across six subjects was painted onto a flattened cortical map of a representative subject. For radial motion, activation was mostly seen in the central representation of V1 (<2°), V2 (<2°), V3 (<5°), and V3A (<5°).

(B) For translation motion, activation was seen in the peripheral V3 (>2°), V3A (>2°), and MT/MST.

(C) Eccentricity map of the representative subject obtained from a separate experiment. The red area in the image indicates voxels that responded maximally when the stimulus was presented in the fovea. The blue and green areas indicate voxels that responded maximally to the parafoveal and peripheral stimuli.

and eccentricity (center < 2°, middle < 5° versus periphery > 5°) was applied to V1, V2, V3, and V3A. A significant interaction between motion type and eccentricity was found in V1 ($p < 0.0001$), V2 ($p < 0.05$), V3 ($p < 0.01$), and V3A ($p < 0.0001$). The results of two-way ANOVA of motion type (translation versus random motion) and eccentricity showed that the interaction between motion type and eccentricity was significant in V3 ($p < 0.05$) and V3A ($p < 0.0001$).

These results were replicated in a control experiment (see Control 1 in the Experimental Procedures) in which the duration of the first and the second intervals varied randomly between 660 and 1320 ms (average duration was kept at 990 ms). This result excludes the possibility that the subjects paid attention to changes in motion speed, which could have been predicted to occur. In addition, because the probability of opponent local motion is higher with the transparent-translation-motion display than with the random-motion display, the higher activity with transparent-translation motion than with the random motion cannot be attributed to opponent suppression [20, 21].

In summary, the central representation of V1, V2, V3, and V3A was activated with radial motion, whereas the peripheral representation of V3A was activated with translation motion, suggesting that differential processing of global motion starts at least in V3A.

In the first experiment, FOE was presented at the center of the visual field. There are at least two possible explanations for the central representation in the low-level areas being more activated with radial motion. The central region of radial-motion stimuli has all directions of motion (all velocities point outward or inward in this region). In addition, the foveal representation in low-level visual areas has smaller receptive fields than more-peripheral representation. Thus, one possibility is that multiple populations of local directionally selective neurons may be excited particularly for the foveal representation because the central region of radial-motion stimuli contains all motion directions. The second possibility is that a specific pattern of radial motion around FOE drives a greater response.

To examine which possibility is plausible, we shifted the location of the FOE from the fixation point in a second experiment. If the activity is highest in the cortical location corresponding to FOE irrespective of whether FOE is presented in the central or peripheral visual field, then this finding would support the second possibility. In contrast, the first possibility does not predict this particular pattern of activity.

In the second experiment, we examined three conditions. In the first condition, FOE was presented at the fovea (the same location as in Experiment 1). In the second condition, FOE was shifted away by 4.5°. In the third condition, random motion was presented. The three conditions were alternated in a random order. The other aspects of the procedure were identical to the procedure used in Experiment 1.

As shown in Figure 4, when FOE was presented in the fovea, the pattern of results was very similar to the results for the radial-motion condition in Experiment 1. On the other hand, when FOE was presented in the 4.5° eccentricity (indicated as "the middle" in the figure), no particular signal enhancement was observed in V1,

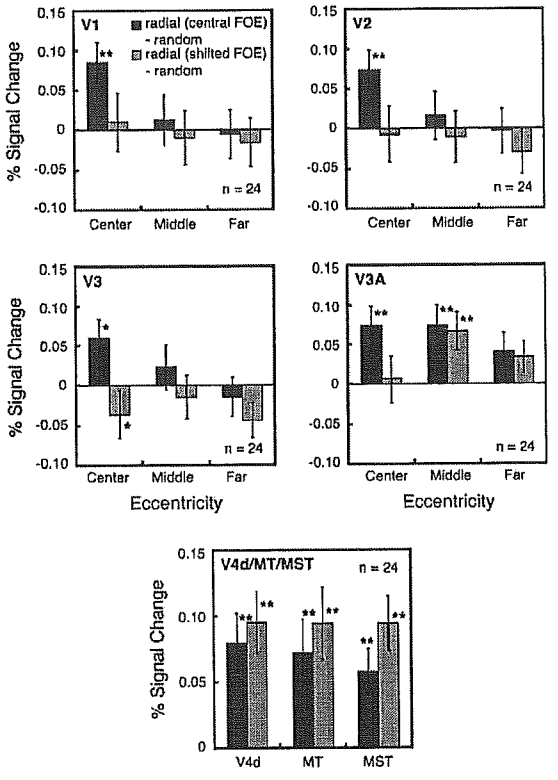

Figure 4. The Results from Experiment 2, in which Expansion and Contraction Were Superimposed

FOE was presented either in the fixation (red) or 4.5° away from the fixation (blue). For purposes of simplicity, we will use the term FOE to refer to the focus of expansion as well as the focus of contraction. For the central FOE condition, radial motion produced significantly stronger MR signals than random motion in the following visual areas: central V1 ($p < 0.01$), central V2 ($p < 0.01$), central V3 ($p < 0.05$), central and middle V3A ($p < 0.01$), V4d ($p < 0.01$), MT ($p < 0.01$) and MST ($p < 0.01$). For the shifted FOE condition, on the other hand, radial motion produced significantly stronger MR signals than random motion only in the middle V3A ($p < 0.01$), V4d ($p < 0.01$), MT ($p < 0.01$), and MST ($p < 0.01$). Note that the strongest activity in V3A was observed in the middle representation when the FOE was presented at 4.5° eccentricity.

V2, and V3 as compared with the random-motion display. In V3A, however, only the representation corresponding to FOE (V3A middle) responded with a significantly greater signal to radial motion than to random motion ($p < 0.001$).

The results indicate that an excited location of V3A depends on the location of the FOE in the visual field. These results cannot be explained by the hypothesis that in Experiment 1 the foveal representation of V3A was excited because local units for multiple directions at the fovea were excited when radial motion was presented in the center. The results are consistent with the hypothesis that V3A responds most strongly to FOE, irrespective of where in the FOE is presented in the visual field.

Two other issues might account for the present results. First, in the speed-discrimination task, the spatial distribution of attention may vary as a function of retinal location and motion type. Specifically, subjects might perform the task with greater attention to FOE in the central regions of the visual field for radial-motion display, whereas they might have greater attention to more-peripheral regions for global-flow motion display. A second concern is that in the main experiment, the direction of the translation motion switched among four alternatives every 4 s, whereas for the radial-motion pattern, the stimuli switched between two alternatives (expansion and contraction). This concern raises the possibility that adaptation effects had differential roles in the two types of motion displays.

To examine these issues, we conducted a third experiment with three conditions. In the first and second conditions, radial motion was presented with FOE at the fixation point and 4.5° shifted away from the fixation point, respectively. In the third condition, transparent-translation displays were used. For avoiding the possibility that subjects directed attention differently to the different types of motion, a control task was performed. During presentation of a motion display, for the first 500 ms in every 1 s, subjects (who had not participated in the previous experiments) were presented with a pale red dot in a location that was randomly chosen in each presentation or with nothing, and they were instructed to press a button depending on whether a dot was presented or not within the remaining 500 ms interval (see Experimental Procedures). This manipulation ensured that attention was not directed to any particular place [10, 30]. For avoiding adaptation effects, the direction of the translation motion was switched between two alternatives—similar to the radial-motion display. Thus, in each display, two opposite ranges of directions covering 90° were presented in an alternating pattern.

The results indicated two important findings. First, the location of V3A that corresponds to FOE was significantly more activated with the radial-motion display than with random motion when the FOE was presented in the center ($p < 0.0001$) and at the 4.5° eccentricity location ($p < 0.001$). Second, the peripheral representation of V3A was more significantly activated with the translation-motion display than random motion ($p < 0.0001$). Thus these results rule out the aforementioned attention and adaptation issues.

A well-established view of motion processing in the monkey brain is that motion signals processed at low-level cortical areas, including V1, involve the recovery of local-motion signals regardless of the type of global motion; sensitivity to different motion patterns becomes different at higher extrastriate areas such as MST [1, 31, 32]. However, our fMRI results with humans are in accord with the hypothesis that in the human brain, differential processing for radial motion and translation motion occurs at V3A, which is lower than MST.

In monkeys, it was well known that MST responds differently to different types of global motion. It has been pointed out that human V3A, which is lower than MST, responds to global motion. However, it was not clear whether V3A responds differently to different types of global motion and how it responds to different motion patterns. The present results indicate that V3A responds differently to two different types of global motions—translation motion and radial motion. V3A responds best to FOE irrespective of where it is presented in central or more-peripheral regions of the visual field. On the

other hand, the peripheral representation in V3A responds best to translation motion.

Experimental Procedures

Subjects

The subjects ranged in age between 22 and 38 yr. All subjects (n = 6 in each experiment) had normal or corrected-to-normal vision. One of the subjects was an author, and the other subjects were naive with regard to the purpose of the experiment. Informed consent was obtained from all subjects. The experiment was performed in compliance with relevant laws and the institutional guidelines of Massachusetts General Hospital (#2000P-001155).

Visual Stimulus

Visual stimuli were generated in real time on a Macintosh G4 computer outside the magnet bore. A color LCD projector (Sharp Note Vision 6; 1024 × 768 pixels, 75 Hz) was used to project the image onto a translucent projection screen located near the subject's head inside the bore. The subjects viewed the screen by looking up onto an adjustable mirror that was angled at about 45° to each subject's normal line of sight. The screen size was 27 × 20 cm. A fixation bull's-eye was presented at the center of the screen. The viewing distance (the distance between the display and the mirror and the distance between the mirror and the observer) was 55 cm. There were three types of motion: translation motion, radial, and random. For all motion types, 200 moving dots were presented in a circular aperture, 20.6° in diameter. In all three types of motion displays, the luminance of the dots and the background was 59.8 cd/m^2 and 0 cd/m^2, respectively. The dot density was roughly the same in any region of the display.

In the first experiment, for translation motion, the direction of motion of the dots was within two opponent ranges of 45°, i.e., ±22.5° from the mean direction. The mean direction pairs were (0° and 180°), (45° and 225°), (90° and 270°), and (135° and 315°). During one epoch of 16 s, the mean directions of dots switched every 4 s, so that 360° motion directions were covered in an epoch. For radial motion, dots moved outward (expansion) or inward (contraction). During one epoch of 16 s, the directions of dots (expansion or contraction) switched randomly every 4 s. The motion directions of the dots covered 360°. For random motion, each dot moved in a random direction within a 360° range. In the three motion displays, the dots traveled at two speeds (see Attentional-Control Task below). Dots traveled 0.4° from one frame to another at the 37.5 Hz frame rate (=15°/s) in the slower motion display; in the faster display, the speed increased by 6%–20%, depending on the subject's performance. The lifetime of each dot was 6 frames (=160 ms).

In the second experiment, FOE was presented either at the fovea, as in the previous experiment, or at 4.5° eccentricity. One hundred expanding dots and 100 contracting dots were superimposed, so that both motion-pattern directions were perceived at the same time simultaneously to equate with the global-motion display in the first experiment.

In the third experiment, transparent-translation motion (identical to those used in Experiment 1) and radial motion displays—one with the focus at the fovea and the other with the focus at the 4.5° eccentricity (identical to Experiment 2)—were used.

Experimental Design

One run consisted of four sets of three epochs in Experiments 1 and 2 and of four sets of four epochs in Experiment 3, and each epoch consisted of four trials of 4 s. In each epoch, a different type of motion was presented. Therefore, the duration of one run was 4 s × 4 trials × 3 epochs × 4 sets = 192 s in Experiments 1 and 2 and 4 s × 4 trials × 4 epochs × 4 sets = 256 s in Experiment 3. The order of the presentation of the three types of motion displays was randomized within a set, and the direction of translation motion and radial motion was randomized within an epoch. Twelve runs were conducted for each subject.

Attention-Control Task

Two well-established methods to control attention were used [22, 23]. On each trial of Experiments 1 and 2, the subject viewed the motion stimulus for 1980 ms. The speed of the dots changed in the middle of the trial, by 6%–20% depending on the subject's performance. The subject judged whether the dots moved faster in the first or second interval by responding with a key-press. The response was made within 2020 ms following the stimulus display. We also conducted a control experiment in which the duration of the first and the second intervals varied randomly between 660 and 1320 ms while the other parameters remained the same. On each trial of Experiment 3, for the first 500 ms in every 1 s, a red stationary dot was presented or no such dot was presented. The subjects were asked to push a button depending on whether the dot was presented or not during the remaining 500 ms. Subjects' performance was maintained between 65% and 85% accuracy by adjusting the difference in dot speeds between the first and second intervals in Experiments 1 and 2, and by adjusting saturation of the red dot in Experiment 3, respectively.

Imaging Procedures

The subjects were scanned in a 3T scanner with EPI (Siemens 3T Allegra). MR images were acquired by using a custom-built, quadrature-based, semi-cylindrical surface coil, with voxels of 3.125 mm in-plane and 3 mm slice. Each slice was oriented perpendicular to the calcarine sulcus, covering all visual areas in the occipital lobe as well as parietal and temporal regions.

Data Analysis

The boundaries of each visual area for each subject were defined in a separate experiment with the standardized retinotopic-stimulus method based on the phase maps for eccentricity and polar angle [24, 25]. These objectively defined borders were available for visual areas V1 (superior and inferior), V2 (superior and inferior), V3/VP, V3A, V4d, and V4v. The locations of MT and MST were defined by the method developed by Huk et al. [26]. In the main experiment, the images from each subject were motion corrected and smoothed with a Gaussian filter of 6 mm FWHM, by using FreeSurfer (http://surfer.nmr.mgh.harvard.edu/). Time-course data for all voxels within a functionally defined ROI (regions of interest), such as V1-center, were averaged for each hemisphere for each subject. These data were normalized for each subject as percent signal change from the mean activation of all the voxels in the ROI. Normalized time-course data were averaged across subjects. Finally, normalized ROI data were selectively averaged by epochs for each subject and condition.

Acknowledgments

We thank Ione Fine, David Heeger, Alexander Huk, Wim Vanduffel, David Whitney, Erica Whitney, and Keiji Tanaka for their valuable comments on the experiments or early drafts. This study was supported by a JSPS fellowship to S.K., NIH grant (EY R01-07980) to R.T., NIH grant (NIA 2R01AG013419-06A2) to G.J.A., and NSF grant (BCS-9905914, CELEST), NIH grant (R01EY015980-01), and Human Frontier Research grant (RGP18/2004) to T.W.

Received: March 11, 2005
Revised: October 3, 2005
Accepted: October 4, 2005
Published: November 21, 2005

References

1. Tanaka, K., and Saito, H. (1989). Analysis of motion of the visual field by direction, expansion/contraction, and rotation cells clustered in the dorsal part of the medial superior temporal area of the macaque monkey. J. Neurophysiol. *62*, 626–641.
2. Duffy, C.J., and Wurtz, R.H. (1991). Sensitivity of MST neurons to optic flow stimuli. I. A continuum of response selectivity to large-field stimuli. J. Neurophysiol. *65*, 1329–1345.
3. Felleman, D.J., and Van Essen, D.C. (1991). Distributed hierarchical processing in the primate cerebral cortex. Cereb. Cortex *1*, 1–47.
4. Atchley, P., and Andersen, G.J. (1998). The effect of age, retinal eccentricity, and speed on the detection of optic flow components. Psychol. Aging *13*, 297–308.

5. Burr, D.C., Morrone, M.C., and Vaina, L.M. (1998). Large receptive fields for optic flow detection in humans. Vision Res. *38*, 1731–1743.
6. Warren, W.H., and Kurtz, K.J. (1992). The role of central and peripheral vision in perceiving the direction of self-motion. Percept. Psychophys. *51*, 443–454.
7. Warren, W.H.J. (1998). The State of Flow. In High-level motion processing, T. Watanabe, ed. (Cambridge, MA: MIT Press), pp. 315–158.
8. Tanaka, K. (1998). Representation of Visual Motion in the Extrastriate Visual Cortex. In High-level motion processing, T. Watanabe, ed. (Cambridge, MA: MIT Press), pp. 295–313.
9. Tootell, R.B., Mendola, J.D., Hadjikhani, N.K., Ledden, P.J., Liu, A.K., Reppas, J.B., Sereno, M.I., and Dale, A.M. (1997). Functional analysis of V3A and related areas in human visual cortex. J. Neurosci. *17*, 7060–7078.
10. Vanduffel, W., Fize, D., Peuskens, H., Denys, K., Sunaert, S., Todd, J.T., and Orban, G.A. (2002). Extracting 3D from motion: Differences in human and monkey intraparietal cortex. Science *298*, 413–415.
11. Braddick, O.J., O'Brien, J.M., Wattam-Bell, J., Atkinson, J., and Turner, R. (2000). Form and motion coherence activate independent, but not dorsal/ventral segregated, networks in the human brain. Curr. Biol. *10*, 731–734.
12. Braddick, O.J., O'Brien, J.M., Wattam-Bell, J., Atkinson, J., Hartley, T., and Turner, R. (2001). Brain areas sensitive to coherent visual motion. Perception *30*, 61–72.
13. Vaina, L.M., Gryzwacz, N.M., Saiviroonporn, P., LeMay, M., Bienfang, D.C., and Cowey, A. (2003). Can spatial and temporal motion integration compensate for deficits in local motion mechanisms? Neuropsychologia *41*, 1817–1836.
14. Williams, D.W., and Sekuler, R. (1984). Coherent global motion percepts from stochastic local motions. Vision Res. *24*, 55–62.
15. Watamaniuk, S.N., Sekuler, R., and Williams, D.W. (1989). Direction perception in complex dynamic displays: The integration of direction information. Vision Res. *29*, 47–59.
16. Treue, S., Hol, K., and Rauber, H.J. (2000). Seeing multiple directions of motion-physiology and psychophysics. Nat. Neurosci. *3*, 270–276.
17. Watanabe, T., Nanez J.E., Sr., Koyama, S., Mukai, I., Liederman, J., and Sasaki, Y. (2002). Greater plasticity in lower-level than higher-level visual motion processing in a passive perceptual learning task. Nat. Neurosci. *5*, 1003–1009.
18. Morrone, M.C., Tosetti, M., Montanaro, D., Fiorentini, A., Cioni, G., and Burr, D.C. (2000). A cortical area that responds specifically to optic flow, revealed by fMRI. Nat. Neurosci. *3*, 1322–1328.
19. Rees, G., Friston, K., and Koch, C. (2000). A direct quantitative relationship between the functional properties of human and macaque V5. Nat. Neurosci. *3*, 716–723.
20. Snowden, R.J., Treue, S., Erickson, R.G., and Andersen, R.A. (1991). The response of area MT and V1 neurons to transparent motion. J. Neurosci. *11*, 2768–2785.
21. Heeger, D.J., Boynton, G.M., Demb, J.B., Seidemann, E., and Newsome, W.T. (1999). Motion opponency in visual cortex. J. Neurosci. *19*, 7162–7174.
22. Huk, A.C., and Heeger, D.J. (2000). Task-related modulation of visual cortex. J. Neurophysiol. *83*, 3525–3536.
23. Huk, A.C., and Heeger, D.J. (2002). Pattern-motion responses in human visual cortex. Nat. Neurosci. *5*, 72–75.
24. Engel, S.A., Glover, G.H., and Wandell, B.A. (1997). Retinotopic organization in human visual cortex and the spatial precision of functional MRI. Cereb. Cortex *7*, 181–192.
25. Sereno, M.I., Dale, A.M., Reppas, J.B., Kwong, K.K., Belliveau, J.W., Brady, T.J., Rosen, B.R., and Tootell, R.B. (1995). Borders of multiple visual areas in humans revealed by functional magnetic resonance imaging. Science *268*, 889–893.
26. Huk, A.C., Dougherty, R.F., and Heeger, D.J. (2002). Retinotopy and functional subdivision of human areas MT and MST. J. Neurosci. *22*, 7195–7205.
27. Tootell, R.B., and Hadjikhani, N. (2001). Where is 'dorsal V4' in human visual cortex? Retinotopic, topographic and functional evidence. Cereb. Cortex *11*, 298–311.
28. Press, W.A., Brewer, A.A., Dougherty, R.F., Wade, A.R., and Wandell, B.A. (2001). Visual areas and spatial summation in human visual cortex. Vision Res. *41*, 1321–1332.
29. Van Oostende, S., Sunaert, S., Van Hecke, P., Marchal, G., and Orban, G.A. (1997). The kinetic occipital (KO) region in man: An fMRI study. Cereb. Cortex *7*, 690–701.
30. Sasaki, Y., and Watanabe, T. (2004). The primary visual cortex fills in color. Proc. Natl. Acad. Sci. USA *101*, 18251–18256.
31. Movshon, J.A., and Newsome, W.T. (1996). Visual response properties of striate cortical neurons projecting to area MT in macaque monkeys. J. Neurosci. *16*, 7733–7741.
32. Andersen, R.A. (1997). Neural mechanisms of visual motion perception in primates. Neuron *18*, 865–872.

Correlation Between Quantitative-EEG Alterations and Age in Patients With Interferon-α–Treated Hepatitis C

Satoshi Kamei, Kentaro Oga,† Masato Matsuura,‡ Naohide Tanaka,§ Takuya Kojima,‡ Yasuyuki Arakawa,§ Yoshihiro Matsukawa,‖ Tomohiko Mizutani,* Teiichiro Sakai,‡ Hitoshi Ohkubo,¶ Hiroshi Matsumura,† Mitsuhiko Moriyama,§ and Kaname Hirayanagi#*

Abstract: The authors recently observed alterations in the quantitative EEG findings in patients with chronic hepatitis C who were treated with interferon-α (IFN-α). However, the factors that influenced such EEG alterations remain unclear. The authors evaluated the correlation between QEEG alterations that occurred during IFN-α treatment and the age of 98 patients with chronic hepatitis C. These patients underwent blind, prospective, and serial quantitative EEG examinations. IFN-α was administered intramuscularly at 9×10^6 IU daily for the first 4 weeks and then three times per week for the next 20 weeks. Serial EEGs were obtained before, at 2 and 4 weeks, and at 2 to 3 days after the treatment. The absolute powers of each frequency band at different stages of the treatment were determined by QEEG. The ages of the patients were classified into five groups: 20 to 29, 30 to 39, 40 to 49, 50 to 59, and ≥60 years. The relationship between the alterations in power values and age was statistically evaluated. As the age of the patients increased, the alterations in power values for the slow waves, alpha 2, and fast waves during IFN-α treatment became more remarkable, and significant (repeated-measure analysis of variance; $P < 0.0001$). The alterations of EEG occurring during IFN-α treatment were marked in older patients.

Key Words: Interferon-α, Quantitative EEG, Chronic hepatitis C, Age of patient.

(*J Clin Neurophysiol* 2005;22: 49–52)

Departments of *Neurology and ‡Neuropsychiatry, §Third Department of Internal Medicine, and ‖First Department of Internal Medicine, Nihon University Itabashi Hospital; Departments of †Neuropsychiatry and ¶Internal Medicine, Nihon University Surugadai Hospital; †Department of Internal Medicine, Itabashi Medical Association Hospital; and #Department of Hygiene and Public Health, Nihon University of Physical Education, Tokyo, Japan

This study was supported by a grant from the Ministry of Education, Culture, Sports, Science, and Technology for the promotion of the industry–university collaboration at Nihon University, Japan.

Address correspondence and reprint requests to Dr. Satoshi Kamei, Department of Neurology, Nihon University School of Medicine, 30–1 Oyaguchi-kamimachi, Itabashi-ku, Tokyo 173–8610, Japan; e-mail: skamei@med.nihon-u.ac.jp.

ISSN: 0736-0258/05/2201-0049

Alterations of brain waves on EEGs during treatment with interferon-α (IFN-α) have been described in several case reports (Meyers et al., 1991; Rohatiner et al., 1983; Smedley et al., 1983). We recently confirmed a diffuse slowing based on an analysis of blind, prospective, and serial quantitative-EEG (QEEG) examinations undertaken in many patients with IFN-α–treated chronic hepatitis C (Kamei et al., 1999). We speculated that such diffuse slowing on the EEGs could reflect a mild adverse effect on the brain caused by the IFN-α treatment. We also reported that this alteration of the quantitative EEG was clinically related to the change in score on the Mini-Mental State Examination (Kamei et al., 2002). However, no detailed investigations on clinical factors that may influence such EEG alterations during IFN-α treatment have yet been made. The present study is the first to evaluate the relationship between the alterations of quantitative EEG that occur during IFN-α treatment and the age of the patient.

SUBJECTS AND METHODS

Subjects

The subjects consisted of 98 previously reported patients with chronic hepatitis C who underwent our blind, prospective, and serial QEEG examinations (Kamei et al., 1999) during the period from August 1995 to May 2003. These patients were independently registered at three different hospitals (Nihon University Itabashi Hospital, Nihon University Surugadai Hospital, and Itabashi Medical Association Hospital) during this period. All patients had been investigated and treated under the same clinical regimen and conditions, including the diagnostic criteria, QEEG examinations, and IFN-α treatment, as reported previously (Kamei et al., 1999). The clinical diagnosis of chronic hepatitis C was confirmed on the basis of serologic findings of serum antibody for hepatitis C virus, histopathologic findings obtained by liver biopsy, detection of the viral genome sequence for hepatitis C virus by the reverse-transcriptase polymerase chain reaction, serum liver function tests, and the clinical course of the patients. IFN-α was administered intramuscu-

larly at a dose of 9×10^6 IU daily for the first 4 weeks and then three times per week for the following 20 weeks under an identical regimen of IFN-α treatment. Informed consent to perform the present study was obtained from all patients. The values for the serologic hepatic function of the 98 patients improved during IFN-α treatment. The means and standard deviations for the values of aspartate aminotransferase (AST/GOT) (normal: 8–38 IU/L) were 126.2 ± 75.1 IU/L before treatment, 50.7 ± 23.6 IU/L at 2 weeks of treatment, 43.2 ± 24.1 IU/L at 4 weeks of treatment, and 40.4 ± 23.1 IU/L after treatment. The values for alanine aminotransferase (ALT/GPT) (normal: 4–44 IU/L) were 164.1 ± 93.2 IU/L before treatment, 60.4 ± 33.2 IU/L at 2 weeks of treatment, 55.0 ± 29.1 IU/L at 4 weeks of treatment, and 52.4 ± 27.1 IU/L after treatment. No patient displayed elevation of serologic hepatic function during IFN-α treatment.

Quantitative-EEG Analysis

The EEG recordings and QEEG analysis used in the present study were described previously (Kamei et al., 1999). Briefly, serial EEGs were obtained before IFN-α treatment, at 2 and 4 weeks of treatment, and at 2 to 3 days after the treatment. The serial EEGs at 2 and 4 weeks of treatment were examined during the period from 1 to 6 hours after the injection of IFN-α. The EEGs in each subject were recorded on a magnetic optical disk from 16 electrode locations according to the international 10–20 system using a digital EEG instrument (Neurofax EEG-4518; Nihon Kohden, Tokyo, Japan). The EEGs were referenced to the ipsilateral earlobes. Sixty seconds of QEEG data were selected visually from each subject and digitized at 128 Hz with a time constant of 0.3 by using a high-frequency filter of 60 Hz. Thirty epochs with a duration of 2 seconds were collected from the subsequent resting period during which time the subjects'eyes were closed for QEEG analysis. The analytical procedure involved the application of fast-Fourier transformation of the collected EEG signals by Rhythm 10.0 (Stellate Systems Inc, Montreal, Quebec, Canada). The frequency ranges were divided into six bands: delta (1.17–3.91 Hz), theta 1 (4.30–5.86 Hz), theta 2 (6.25–7.81 Hz), alpha 1 (8.20–10.16 Hz), alpha 2 (10.55–12.89 Hz), and beta (13.28–30.86 Hz). The absolute powers of each frequency band were calculated at each electrode location in each subject. Each power value was obtained by integrating the appropriate part of the spectrum. The present quantitative analysis was carried out blindly during routine EEG work involving many other disease states, including epilepsy, cerebrovascular disease, encephalitis, meningitis, metabolic encephalopathy, and brain tumor, as well as in normal controls. The only knowledge that the EEG analyst (S.K.) possessed regarding each patient was the his or her identification number, and he did not therefore have any other information concerning any of the studied subjects such as their clinical diagnosis, date of treatment, or kind of treatment.

Statistical Analysis

In June 2004, the statistical analyst (K.H.) collected the QEEG-analyzed data for the 98 subjects and information about the ages of the patients at another independent institute. The patients'ages were classified into five groups: 20 to 29, 30 to 39, 40 to 49, 50 to 59, and ≥60 years. The distributions of the power values at each frequency band for each electrode location were evaluated in terms of their skewness and kurtosis. According to the data obtained for the skewness and kurtosis, repeated-measure analysis of variance (ANOVA) was applied to the alterations in power values as the main factor among four different periods: before the IFN-α treatment, at 2 and at 4 weeks of treatment, and after the treatment, with the frequency bands, electrode locations, and patients'age classifications as cofactors. the statistical software StatView 5 (Abacus Concepts, Berkeley, CA, U.S.A.) was used. The QEEG variables were evaluated in relation to patient age by post hoc analysis of variance (Scheffé test). Probability values of less than 0.05 were considered as significant.

RESULTS

The 98 subjects ranged in age from 23 to 70 years (mean ± SD: 47.9 ± 10.6 years). The results of the serial QEEG studies for each selected frequency of EEG during the IFN-α treatment in each age group are summarized in Fig. 1. Increased slow waves (delta, theta 1 and 2) and decreased alpha 2 and beta waves were evident during the IFN-α treatment in all age groups. Such EEG alterations during the IFN-α treatment in the present blind, prospective, multicenter controlled study confirmed our previous observations (Kamei et al., 1999). Moreover, the alterations in power values during the IFN-α treatment became more remarkable as the patients'age increased. Statistical data for the analysis of the alterations in power values and ages obtained by the repeated-measure ANOVAs and post hoc ANOVAs are presented in Tables 1 and 2. The repeated-measure ANOVA results for the alterations in power values revealed a significant difference between the alteration in power values during the treatment and either the patients'age or frequency band (both $P < 0.0001$). The post hoc ANOVA results indicated that there were significant differences in the alterations of absolute power values during the IFN-α treatment for all comparisons with increasing patient ages in the case of the delta, theta 1, and beta waves, except for several comparisons with only 10-year alterations of age group. There were no significant differences in the alterations of power values during the IFN-α treatment in the case of the alpha 1 and total power values.

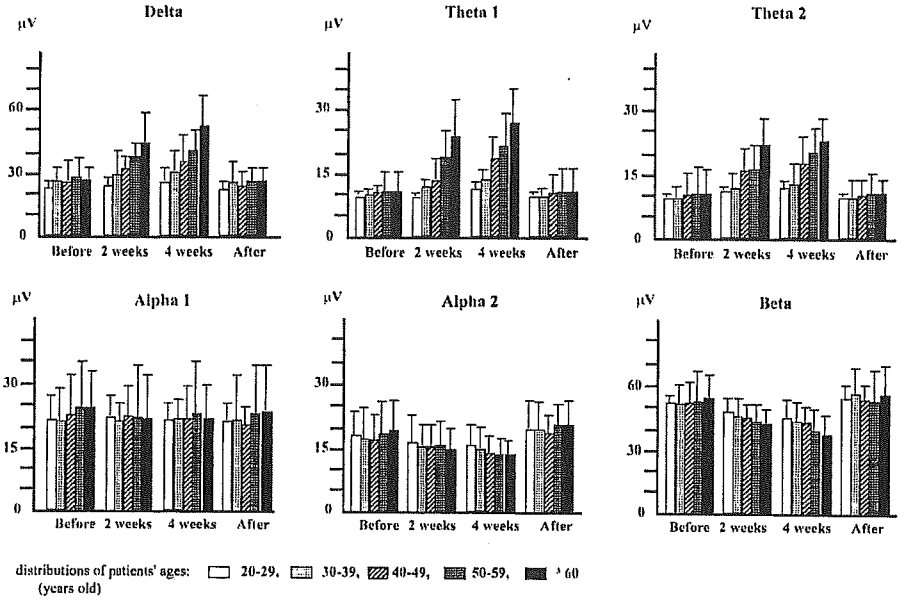

FIGURE 1. Alterations in absolute power values (mean ± SD) with changes of patients'age for each frequency band at before IFN-α treatment, at 2 and at 4 weeks after treatment, and at 2 to 3 days after treatment. Increasing power values in the slow waves (delta, theta 1 and 2) and decreasing power values in the alpha 2 and beta waves during IFN-α treatment, in comparison with those observed before and after IFN-α treatment, were evident for all age classifications. Moreover, the alterations in power values became more remarkable with increasing age in all frequency bands except for the alpha 1 and total power values.

TABLE 1. Repeated-measure Analysis of Variances Between Alterations in Power Values During IFN-α Treatment and Patient Age

Factors	
Alteration of power values during IFN-α treatment (Alteration of power values)	$P < 0.0001$ ($F = 30.338$)
Alteration of power values × Difference of patients' ages (Difference of age)	$P < 0.0001$ ($F = 16.081$)
Alteration of power values × Frequency bands	$P < 0.0001$ ($F = 48.781$)
Alteration of power values × Electrode location	NS
Alteration of power values × Difference of age × Frequency bands × Electrode location	NS

NS, not significant; x, interaction.

DISCUSSION

Although many patients have undergone IFN-α treatment, controlled detailed assessments of the adverse effects of IFN-α on the function of the central nervous system have not yet been described. Evaluations of brain functional alterations have been given in only three previous reports based on data from small numbers of patients who received EEG examinations (Meyers et al., 1991; Rohatiner et al., 1983; Smedley et al., 1983). We recently confirmed a significant, diffuse slowing on QEEGs that occurred in chronic hepatitis C patients during IFN-α treatment at a relatively low dosage (Kamei et al., 1999). At such a low dosage of IFN-α administration to chronic hepatitis C patients, the diffuse slowing of the EEG is reversible after completion of the treatment (Kamei et al., 1999). However, in one previous case report involving a high dosage of IFN-α, the alteration in the EEG was found to be persistent (Meyers et al., 1991). Moreover, neuropsychiatric complications have been described as difficult to evaluate after IFN-α treatment in patients with chronic viral hepatitis (Saracco and Rizzetto, 1999). In view of the considerable numbers of patients undergoing IFN-α treatment, detailed knowledge of the factors that influence EEG alterations due to IFN-α treatment is important for practicing physicians to predict the appearance of such adverse effects on brain function after IFN-α treatment. The results obtained in present study indicate that patient age is one of the factors that influence the alteration in EEGs during IFN-α treatment. Serial monitoring by EEG is thus considered to be of value for detecting alterations of brain function during IFN-α treatment in chronic viral hepatitis patients, and the alterations in the serial EEGs should be monitored carefully, particularly in older patients.

CONCLUSION

We evaluated the correlation between QEEG alterations that occurred during IFN-α treatment and the age of patients with chronic hepatitis C. A total of 98 patients with chronic hepatitis C underwent blind, prospective, and serial

TABLE 2. Statistical Comparisons of Alterations in Power Values During IFN-α Treatment for Each Frequency Band Among Each of the Patient's Age Distributions, by Post Hoc ANOVAs

Comparison of Different Age Distributions	Power Values (μV)						
	Delta	Theta 1	Theta 2	Alpha 1	Alpha 2	Beta	Total
G2 vs. G3	*	†	NS	NS	NS	†	NS
G2 vs. G4	*	*	*	NS	†	*	NS
G2 vs. G5	*	*	*	NS	*	*	NS
G2 vs. G6	*	*	*	NS	*	*	NS
G3 vs. G4	†	†	†	NS	NS	NS	NS
G3 vs. G5	*	*	*	NS	†	†	NS
G3 vs. G6	*	*	*	NS	†	*	NS
G4 vs. G5	*	*	†	NS	NS	†	NS
G4 vs. G6	*	*	*	NS	†	*	NS
G5 vs. G6	*	*	*	NS	NS	†	NS

Distributions of patients' ages (years old): G2 = 20–29, G3 = 30–39, G4 = 40–49, G5 = 50–59, G6 ≥ 60.
*$P < .01$.
†$P < .05$.
NS, not significant.

QEEG examinations at three independent hospitals. Our results show that the EEG alterations observed during IFN-α treatment in patients with chronic hepatitis C became more remarkable as the age of the patients increased.

REFERENCES

Kamei S, Tanaka N, Matsuura M, Arakawa Y, Kojima T, Matsukawa Y, Takasu T, Moriyama M. (1999) Blinded, prospective, and serial evaluation by quantitative-EEG in interferon-alpha-treated hepatitis-C. *Acta Neurol Scand* 100:25–33.

Kamei S, Sakai T, Matsuura M, Tanaka N, Kojima T, Arakawa Y, Matsukawa Y, Mizutani T, Oga K, Ohkubo H, Matsumura H, Hirayanagi K. (2002) Alterations of quantitative EEG and Mini-Mental State Examination in interferon-α-treated hepatitis C. *Eur Neurol* 48:102–7.

Meyers CA, Scheibel RS, Forman AD. (1991) Persistent neurotoxicity of systemically administered interferon-alpha. *Neurology* 41:672–6.

Rohatiner AZS, Prior PF, Burton AC, Smith AT, Balkwill FR, Lister TA. (1983) Central nervous system toxicity of interferon. *Br J Cancer* 47:419–22.

Saracco G, Rizzetto M. Therapy of chronic viral hepatitis. In: Bircher J, Benhamou J-P, McIntyre N, Rizzetto M, Rodés J, eds. *Oxford textbook of clinical hepatology*. Vol 1, 2nd ed. Oxford: Oxford University Press, 1999:939–54.

Smedley H, Kartrak M, Sikora K, Wheeler T. (1983) Neurological effects of recombinant interferon. *BMJ* 286:262–4.

Abnormal Regional Cerebral Blood Flow in Systemic Lupus Erythematosus Patients With Psychiatric Symptoms

Kenji Oda, M.D., Ph.D.; Eisuke Matsushima, M.D., Ph.D.; Yoshiro Okubo, M.D., Ph.D.; Katsuya Ohta, M.D., Ph.D.; Yuji Murata, M.D., Ph.D.; Ryuji Koike, M.D., Ph.D.; Nobuyuki Miyasaka, M.D., Ph.D.; and Motoichiro Kato, M.D., Ph.D.

Objective: Single-photon emission computed tomography (SPECT) studies have demonstrated decreased regional cerebral blood flow (rCBF) in systemic lupus erythematosus (SLE) patients. However, no study has done voxel-based analysis using statistical parametric mapping (SPM) that can evaluate rCBF objectively, and the relationship between rCBF and psychiatric symptoms has not been well investigated. Using L,L-ethyl cysteinate dimer (^{99m}Tc ECD) SPECT and SPM, we aimed to clarify the association of rCBF changes with psychiatric symptoms in SLE patients whose magnetic resonance imaging (MRI) showed no morphological abnormalities.

Method: Twenty SLE patients and 19 healthy volunteers underwent ^{99m}Tc ECD SPECT. Data were collected from August 2000 to March 2003. SLE was diagnosed according to American College of Rheumatology criteria, and psychiatric symptoms were diagnosed according to ICD-10 criteria. On the basis of the modified Carbotte, Denburg, and Denburg method, the patients were classified into 3 groups: a group with major psychiatric symptoms (hallucinosis, delusional disorder, and mood disorder), a group with minor psychiatric symptoms (anxiety disorder, dissociative disorder, and emotionally labile disorder), and a group without psychiatric symptoms. Gross organic lesions were ruled out by brain MRI. Group comparisons of rCBF were performed with analysis using SPM99.

Results: SLE patients without MRI lesions showed decreased rCBF in the posterior cingulate gyrus and thalamus. The reduction in rCBF was overt in patients with major psychiatric symptoms.

Conclusion: Our study indicated that SLE patients may have dysfunction in the posterior cingulate gyrus and thalamus and that this may be associated with the severity of psychiatric symptoms.

(J Clin Psychiatry 2005;66:00–00)

Received Sept. 13, 2004; accepted Jan. 10, 2005. *From the Section of Liaison Psychiatry and Palliative Medicine (Drs. Oda, Matsushima, and Ohta), Section of Diagnostic Radiology and Oncology (Dr. Murata), and Department of Bioregulatory Medicine and Rheumatology (Drs. Koike and Miyasaka), Graduate School of Tokyo Medical and Dental University, Tokyo, Japan; Onda-daini Hospital, Chiba, Japan (Drs. Oda and Ohta); Department of Neuropsychiatry, Nippon Medical School, Tokyo, Japan (Dr. Okubo); and Department of Neuropsychiatry, Keio University School of Medicine, Tokyo, Japan (Dr. Kato).*

This work was supported by a Grant-in-Aid for Scientific Research from the Ministry of Education, Culture, Sports, Science and Technology, Tokyo, Japan, and a research grant for nervous and mental disorders from the Ministry of Health, Labor and Welfare of Japan, Tokyo (11B-3).

Asako Emori, M.A., Hiroshi Onda, M.D., Ph.D., Tetsuya Suhara, M.D., Ph.D., Tetsuya Ichimiya, M.D., Ph.D., and the staffs of Onda-daini Hospital and the Brain Imaging Project, National Institute of Radiological Sciences, Chiba, Japan, are gratefully acknowledged.

Corresponding author and reprints: Eisuke Matsushima, M.D., Ph.D., Section of Liaison Psychiatry and Palliative Medicine, Graduate School of Tokyo Medical and Dental University, 1-5-45, Yushima, Bunkyo-ku, Tokyo 113-8519, Japan (e-mail: em.lppm@tmd.ac.jp).

Systemic lupus erythematosus (SLE) is an autoimmune disease with a variety of clinical features including abnormalities of the skin, joints, lungs, heart, kidneys, and central nervous system (CNS). CNS involvement is one of the important manifestations of SLE and is variously reported to occur in 20% to 75% of SLE patients.[1–5] The features of neuropsychiatric symptoms vary from global to focal cerebral dysfunction,[5,6] and the occurrence of not only neurologic diseases such as cerebrovascular disease, seizures, headaches, dizziness, and cognitive disorders, but also psychiatric symptoms such as hallucination, delusion, mood disorder, anxiety disorder, dissociative disorder, emotionally labile disorder, etc., have been reported.[7,8] However, the pathophysiology underlying CNS diseases has remained elusive.[8] The observation of both diffuse and focal CNS involvements in SLE has led to the hypothesis that there are several pathogenic mechanisms in these patients such as microvascular damage, small vessel vasculopathy, and autoantibody-mediated neuronal cell injury.[9–12] Many studies have already been performed with neuroimaging technologies such as magnetic resonance imaging (MRI) and single-photon emission computed tomography (SPECT). Several studies have reported that brain T2-weighted MRI is

sensitive for the detection of CNS lesions, i.e., a wide spectrum of MRI abnormalities has been described in such patients, including isolated and multiple ischemic lesions, dural sinus thrombosis, brain atrophy, and diffuse meningeal thickening.[13–21]

Cerebral blood flow (CBF) imaging techniques using ^{133}Xe blood flow or SPECT have also been applied,[22] proving to be highly sensitive in monitoring CNS involvement in patients with SLE.[23–25] The use of SPECT for studying blood flow can reveal disease progression and lesions most relevant at the time of evaluation and objectify neuropsychiatric manifestations without detectable MRI abnormalities.[26–30] Several CBF studies[12,23,25–30,32–36,37] have reported hypoperfusion in global or regional CBF. However, these past studies are not without shortcomings.

First, in spite of recent developments in neuroimaging data analysis using voxel-based analysis, most of the studies adopted the visual inspection method that is thought to have lower sensitivity, or the region of interest (ROI) method that only provides regional CBF (rCBF) data for a limited portion of the brain where the selected ROIs are located.[31] Second, although several studies have noticed the relationship between blood flow and neuropsychiatric symptoms and suggested that low global or regional CBF was associated with the severity of neuropsychiatric symptoms,[12,23,25–30,32–36,38] the subjects' symptoms included not only psychiatric but also neurologic ones at the same time, and their criteria for diagnosis were not well clarified. Third, morphological imaging such as computed tomography (CT) and MRI has been performed in past CBF studies, but its criteria for abnormalities were in disagreement. The manner of morphological imaging varied from the inclusion of ischemic infarction,[12,35–38] cortical atrophy,[23,34,37,38] dilatation of lateral ventricles,[33] and MRI-defined hyperintensity,[25,28–30,32,33,38] to excluding all morphological abnormalities.[26] That is to say, previous studies were not well controlled in respect to CT and MRI findings.

In the present study using statistical parametric mapping (SPM99), we investigated rCBF of SLE patients with and without psychiatric symptoms but without morphological abnormalities on MRI. We aimed to elucidate the rCBF changes in SLE patients and the pathophysiology for psychiatric symptoms.

METHOD

Subjects

We studied 20 patients (1 man, 19 women; mean ± SD age: 36.4 ± 10.8 years), both inpatients and outpatients, who had been diagnosed with SLE at the Tokyo Medical and Dental University Hospital, Tokyo, Japan. The patients fulfilled the American College of Rheumatology criteria for the diagnosis of SLE[39] with (N = 14; 1 male and 13 female patients; mean age: 37.3 ± 12.0 years) or without (N = 6; all female patients; mean age: 35.7 ± 8.6 years) psychiatric symptoms. Patients with a history of stroke, movement disorder, or dementia were excluded. MRIs were performed to rule out gross organic brain lesions (see MRI methods below). Data were collected from August 2000 to March 2003.

A psychiatrist (E.M.) and an accomplished psychologist investigated the psychiatric and mental states of the patients by clinical interview and diagnosed their psychiatric symptoms. Psychiatric symptoms were evaluated on the same day as the SPECT scanning. Then the patients' psychopathologic conditions were reviewed and diagnoses were made by E.M. according to the criteria of ICD-10[40]; patients met the code of F06 for other mental disorders due to brain damage and dysfunction and to physical disease. Patients with psychiatric symptoms were further differentiated into organic hallucinosis (N = 2; ICD-10 code: F06.0), organic delusional (schizophrenia-like) disorder (N = 1; code: F06.2), organic mood (affective) disorder (N = 4; code: F06.3), organic anxiety disorder (N = 4; code: F06.4), organic dissociative disorder (N = 1; code: F06.5), and organic emotionally labile (asthenic) disorder (N = 2; code: F06.6).

Further, on the basis of the modified Carbotte, Denburg, and Denburg method,[41–43] we categorized the patients into 2 groups according to the severity of psychiatric symptoms, i.e., those with major psychiatric symptoms corresponding to hallucinosis, delusional disorder, or mood disorder (N = 7; 1 man and 6 women; mean age: 42.1 ± 10.6 years; code: F06.0, F06.2, or F06.3) and those with minor psychiatric symptoms corresponding to anxiety disorder, dissociative disorder, or emotionally labile disorder (N = 7; all women; mean age: 31.1 ± 9.8 years; code: F06.4, F06.5, or F06.6).

SLE disease activity was evaluated by anti–double-stranded DNA (anti-dsDNA) antibody immunoglobulin G (IgG). The presence of anticardiolipin antibodies (aCL) of IgG and IgM isotypes was determined. If either IgG or IgM index was above 1.0, we considered the patient's aCL as positive. Age, sex, symptom grade, ICD-10 code, psychiatric symptoms, duration of illness, corticosteroid dosage, psychotropic drugs, anti-dsDNA, and aCL were recorded for each patient (Table 1). Age and anti-dsDNA were not significantly different between symptom grades, but duration of illness showed a significant difference between patients with major psychiatric symptoms and without psychiatric symptoms by analysis of variance. Although all but 1 of the patients were receiving corticosteroid treatment, there was no difference in dosage among patients with major psychiatric symptoms, those with minor psychiatric symptoms, and those without psychiatric symptoms.

We also examined 17 female and 2 male age-matched, right-handed, healthy volunteers (mean age: 37.9 ± 8.7 years). They were recruited from the general surrounding

Table 1. Clinical Characteristics of Patients With Systemic Lupus Erythematosus

Patient	Age, y	Sex	Symptom Grade	ICD-10 Code	Symptom	Duration of Illness, y	Steroid Dosage, mg/d	Psychotropic Drug (mg/d)	anti-dsDNA, IU/mL	aCL
1	23	Male	Major	F06.0	Visual hallucination	0	40		< 5	–
2	54	Female	Major	F06.0	Visual hallucination	30	30	Zopiclone (7.5)	64	–
3	53	Female	Major	F06.2	Delusion	40	5		35	–
4	32	Female	Major	F06.3	Major depression	13	12.5		< 5	+
5	39	Female	Major	F06.3	Major depression	0	40	Amoxapine (75)	< 5	+
6	45	Female	Major	F06.3	Bipolar disorder	16	10		11	+
7	49	Female	Major	F06.3	Major depression	1	30		< 5	+
8	16	Female	Minor	F06.4	Anxiety	0	20		< 5	+
9	27	Female	Minor	F06.4	Anxiety	1	35	Trazodone (75)	8	–
10	30	Female	Minor	F06.4	Anxiety	16	5	Milnacipran (50)	114	–
11	37	Female	Minor	F06.4	Anxiety	4	7.5	Estazolam (2)	< 5	–
12	22	Female	Minor	F06.5	Dissociative disorder	2	30	Levomepromazine (10)	6	+
13	39	Female	Minor	F06.6	Emotionally labile disorder	22	7.5	Milnacipran (100)	< 5	–
14	47	Female	Minor	F06.6	Emotionally labile disorder	16	17.5	Lorazepam (3)	< 5	–
15	27	Female	None			0	35		< 5	–
16	33	Female	None			0	30		64	+
17	30	Female	None			4	12.5	Brotizolam (0.25)	< 5	–
18	29	Female	None			2	4		< 5	–
19	48	Female	None			2	0		< 5	+
20	47	Female	None			0	40	Zopiclone (7.5)	7	–

Abbreviations: aCL = anticardiolipin antibodies, anti-dsDNA = anti–double-stranded DNA.
Symbols: – = negative, + = positive.

population, did not meet any criteria for neuropsychiatric disorders, and had no relatives with neuropsychiatric disorders on the basis of unstructured psychiatric screening interviews. Their Mini-Mental State Examination (MMSE)[44] scores were 28 or higher. The volunteers were free of any medication, and they underwent MRI to rule out the presence of any gross organic brain lesions (see MRI methods below).

The purpose and procedures of the study were explained to all subjects, and written informed consent was obtained. This study was approved by the Ethics Committee of Tokyo Medical and Dental University.

Image Acquisition and Analysis

^{99m}Tc ECD (technetium-99m L,L-ethyl cysteinate dimer) SPECT. The consciousness of all subjects at the time of SPECT scanning was clear. They were studied in a supine resting position with eyes closed and minimal sensory simulation in a silent room at the Nuclear Medicine Unit, Tokyo Medical and Dental University Hospital. Brain SPECT was performed using a triple-head gamma camera PRISM 3000 (Picker International, Cleveland, Ohio) with low-energy ultra–high-resolution fan beam collimators. Although most previous SPECT studies used ^{99m}Tc HMPAO (hexamethylpropyleneamineoxime), we used ^{99m}Tc ECD in the present study. The advantages of ^{99m}Tc ECD over ^{99m}Tc HMPAO include a faster blood disappearance rate and more rapid urinary excretion,[45] features resulting in a higher brain-to-background ratio and a lower total-body–absorbed radiation dose. In addition, ^{99m}Tc ECD has a shelf life of approximately 6 hours compared with less than 30 minutes for ^{99m}Tc HMPAO. A bolus of 800 MBq of ^{99m}Tc ECD was injected intravenously from the antecubital vein with a 20-mL saline flush. Scans were performed for 20 minutes, starting precisely 5 minutes after injection. Spatial resolution of the scanner was 3.8 mm full width at half maximum (FWHM). Projection data were acquired in a 128×128 matrix. All SPECT data were reconstructed with a 3D post filter (Butterworth) cutoff frequency of 0.24 cycles/pixel and order 4.0.

MRI. In patients, the whole brain was examined at the Tokyo Medical and Dental University Hospital using a GE 1.5-T MRI camera (General Electric Medical Systems, Milwaukee, Wis.) with a series of T1-weighted images, T2-weighted images, and fluid attenuated inversion recovery (FLAIR) images. MRI scans were assessed by radiologists, and then rechecked by 2 raters (K.O. and E.M.). Patients with cerebral infarction, cortical atrophy, dilatation of lateral ventricles in their MRI, and hyperintensities of more than 2 mm in deep white matter regions or subcortical regions on T2-weighted or FLAIR images were excluded.

In control subjects, MRIs were acquired on a Phillips Gyroscan NT, 1.5-T MRI camera (Phillips, Eindhoven, the Netherlands) with a series of T1-weighted images, T2-weighted images, and proton images at the National Institute of Radiologic Sciences, Chiba, Japan. Their MRI findings were all normal, i.e., none showed cerebral infarction, cortical atrophy, dilatation of lateral ventricles, or even small hyperintensity areas.

Data Analysis

Statistical parametric mapping. We analyzed the data using MATLAB 5.3 (The MathWorks, Natick, Mass.) and SPM99 (Wellcome Department of Cognitive Neurology,

Figure 1. Decreased rCBF in SLE Patients Compared to Controls[a,b]

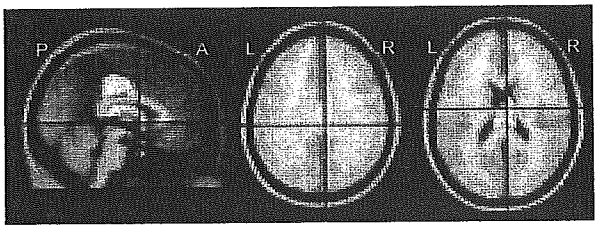

[a]The colored areas show the regions where rCBF decreased significantly in SLE patients compared to controls using SPM99.
[b]Statistically significant differences can be seen on T1 images. Threshold is set at $p < .001$ uncorrected.
Abbreviations: A = anterior, L = left, P = posterior, R = right, SLE = systemic lupus erythematosus, rCBF = regional cerebral blood flow, SPM99 = statistical parametric mapping.

Figure 2. Decreased rCBF in SLE Patients With Major Neuropsychiatric Symptoms Compared to Controls[a,b]

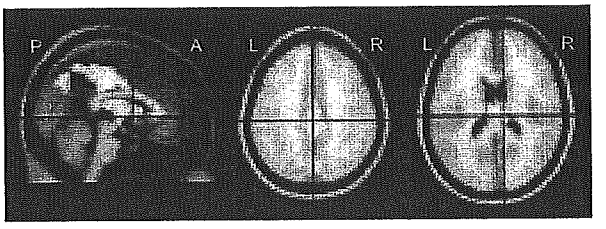

[a]The colored areas show the regions where rCBF decreased significantly in SLE patients compared to controls using SPM99.
[b]Statistically significant differences can be seen on T1 images. Threshold is set at $p < .001$ uncorrected.
Abbreviations: A = anterior, L = left, P = posterior, R = right, rCBF = regional cerebral blood flow, SLE = systemic lupus erythematosus, SPM99 = statistical parametric mapping.

Institute of Neurology, London, U.K.). SPM99 is an increasingly recognized form of neuroimaging analysis for localizing statistically significant changes in spatially normalized images on a voxel-by-voxel basis.[46,47]

Normalization

All converted SPECT images were normalized into the SPM SPECT template, which approximates the standard space of Talairach and Tournoux.[48] The spatial normalization included both affine transformations and a linear combination of smooth spatial $7 \times 8 \times 7$ basis functions that model global nonlinear differences in shape.[49] The spatially normalized structural images (now in stereotactic space) were resliced to a final voxel size of approximately $2 \times 2 \times 2$ mm^3.

Smoothing

Normalized images were smoothed using a 12-mm FWHM isotropic Gaussian kernel. This process conditioned the residuals to conform more closely to the Gaussian random field model underlying the statistical process used for adjusting p values.[46]

Group Comparisons

Group comparisons of rCBF were performed using SPM99, employing the general linear model. Age was covariated, as there was an age effect on rCBF in the regions. Region-specific differences between groups were assessed statistically using a 2-tailed contrast, that is, testing for an increased or decreased probability of a particular voxel. Global CBF was controlled for proportional scanning, and a gray matter threshold of 0.8 was used. In order to examine regional differences, the images were scaled to a mean global CBF of 50 mL/100 g/min. Then the adjusted rCBF images were compared to reveal the relative rCBF distributions in the 2 groups. Thresholds for statistical analysis were set at $p < .001$ uncorrected.

Figure 3. Decreased rCBF in SLE Patients With Minor Neuropsychiatric Symptoms Compared to Controls[a,b]

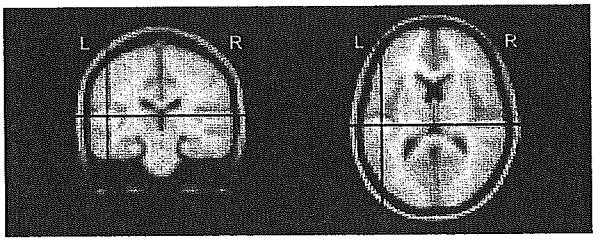

[a]The colored areas show the regions where rCBF decreased significantly in SLE patients compared to controls using SPM99.
[b]Statistically significant differences can be seen on T1 images. Threshold is set at $p < .001$ uncorrected.
Abbreviations: A = anterior, L = left, P = posterior, R = right, rCBF = regional cerebral blood flow, SLE = systemic lupus erythematosus, SPM99 = statistical parametric mapping.

RESULTS

A comparison of the whole SLE patient group (N = 20) and the control group (N = 19) revealed significantly decreased rCBF in the posterior cingulate gyrus and medial dorsal nucleus of the thalamus in SLE patients as shown in Figure 1. The peak Talairach coordinates (x, y, z [mm]) and Z score were (0, –24, 32; Z score = 4.33) and (4, –18, 12; Z score = 4.24), respectively, as shown in Table 2. If the patients were further divided on the basis of their psychiatric symptoms, those with major symptoms also showed decreased rCBF in the posterior cingulate gyrus, thalamus, and precuneus (Figure 2) (peak Talairach coordinates [0, –28, 34; Z score = 4.58], [6, –26, 16; Z score = 4.43], and [2, –74, 26; Z score = 3.76]; Table 2) compared with the control group. The SLE patients with minor psychiatric symptoms showed decreased rCBF in the left superior temporal gyrus and left inferior parietal lobule (Figure 3) (peak Talairach coordinates [–44, –26,

Table 2. Decreased Regional Cerebral Blood Flow in Patients With Systemic Lupus Erythematosus (SLE) (N = 20) Compared to Controls (N = 19)

Variable	Peak Coordinate x	y	z	Region	Z score
SLE < controls	0	−24	32	Posterior cingulate gyrus	4.33
	4	−18	12	Thalamus medial dorsal nucleus	4.24
SLE major psychiatric symptoms < controls	0	−28	34	Posterior cingulate gyrus	4.58
	6	−26	16	Right extra-nuclear	4.43
	2	−74	26	Right precuneus	3.76
SLE minor psychiatric symptoms < controls	−44	−26	8	Left superior temporal gyrus	4.17
	−44	−40	22	Left inferior parietal lobule	3.25

Symbol: < = decreased regional cerebral blood flow in SLE patients compared to controls.

8; Z score = 4.17] and [−44, −40, 22; Z score = 3.25]; Table 2) compared with controls. On the other hand, there was no significant rCBF decrease in the patients without psychiatric symptoms in comparison with the control group. Furthermore, there were no correlations between rCBF and corticosteroid dosage or duration.

DISCUSSION

Many SPECT studies[12,22–30,32–38] have demonstrated decreased CBF in SLE patients. However, most of them were done on the basis of visual inspection or ROI analysis and were not well controlled in terms of brain morphological CT and MRI findings. To the best of our knowledge, this is the first SPECT study using the SPM method to investigate SLE patients. Our results showed reduced rCBF in the posterior cingulate gyrus and thalamus of SLE patients without morphological abnormalities on their MRI, and that this reduction in CBF was related to the severity of their psychiatric symptoms. Although the posterior cingulate gyrus is located in one of the important limbic systems, this region might have been missed in previous studies using ROI analysis.

It is possible that the rCBF decrease is derived from organic change, such as microvascular damage in the brain. Vasculopathy is the major pathogenesis in SLE patients, consisting of the cuffing of small blood vessels in the brain.[3,7,50] This process was formerly attributed to deposition of immune complexes in the walls of these blood vessels, but later the cause of the activation of complement was proposed.[51] Vasculopathy might alter rCBF and result in hypoperfusion of the brain, as has been demonstrated in SPECT studies.[23,25,32–35,37,52,53]

Interestingly, the region including the posterior cingulate gyrus is known to be important for memory.[54] In very early Alzheimer's disease or even in mild cognitive impairment, decreases of rCBF and glucose metabolism in the posterior cingulate gyrus (and precuneus) have been reported in SPECT and positron emission tomography studies.[55–57] Ablation studies suggest that connections between the posterior cingulate gyrus and parahippocampal cortices contribute to spatial orientation, monitoring sensory eye movement and responding to sensory stimuli.[58] On the other hand, the medial dorsal nucleus of the thalamus is suggested to regulate the affective state.[59–61] Insufficiency of this region has a relationship with psychiatric disorders, such as schizophrenia[62–65] and mood (affective) disorder.[59,66]

By comparing patient groups with healthy controls, we were able to clarify the CBF changes in SLE patients. The regions where rCBF reduction was seen in SLE patients partially overlapped with those seen in other neuropsychiatric disorders, such as schizophrenia,[62–65] mood disorder,[59,66] and Alzheimer's disease.[55–57] However, the pattern of rCBF reduction as a whole was assumed to be different from those of other neuropsychiatric diseases. So far as mood disorder was concerned, we examined rCBF using the methodology with the present study and found that depressed patients showed rCBF reduction in the frontal, temporal lobes and anterior cingulate gyrus but not in the posterior cingulate where we found rCBF reduction in SLE patients.[67] Because of the variety of psychiatric symptoms in our SLE patients, it was difficult to gather sufficient "psychiatric" controls and to compare SLE patients with them. However, before we can conclude whether CNS SLE patients can be differentiated from patients with other types of neuropsychopathology, further studies in the use of "psychiatric" controls will be required.

The present study labors under certain limitations. As the number of subjects was small, various psychiatric symptoms were assorted in the same group. Thus, we simply categorized patients into 3 groups according to their psychiatric symptoms using a modified Carbotte, Denburg, and Denburg method. Other limitations may arise from the fact that most patients were receiving various amounts of medications such as corticosteroids, antipsychotic agents, antidepressants, and so on during the study. Regarding corticosteroids, it was reported that their dosage and usage duration are not correlated with rCBF.[68] However, there have been inconsistent findings regarding the effects of antipsychotics[69] and antidepressants[70] on rCBF. Although in this study there was no correlation between rCBF and corticosteroid dosage, and the class and dose of psychotropic drugs seemed to have no influence

on rCBF, a controlled study of the effects of medications is awaited.

In conclusion, using SPECT with ^{99m}Tc ECD and SPM99, we investigated rCBF in SLE patients whose MRIs showed no brain morphological abnormalities from the view of psychiatric symptoms, and we compared the results with the data from controls. The SLE patients showed decreased rCBF in the region containing the posterior cingulate gyrus and thalamus.

Furthermore, a marked reduction in rCBF in this region was seen only in those patients with major psychiatric symptoms. These findings indicate that SLE patients with psychiatric symptoms may have dysfunction in the posterior cingulate gyrus and thalamus, suggesting the possibility of damage in the pathway including the limbic region.

Drug names: estazolam (Prosom and others), lorazepam (Ativan and others), trazodone (Desyrel and others).

REFERENCES

1. Estes D, Christian CL. The natural history of systemic lupus erythematosus by prospective analysis. Medicine (Baltimore) 1971;50:85–95
2. Futrell N, Shultz LR, Millikan C. Central nervous system disease in patients with systemic lupus erythematosus. Neurology 1992;42: 1649–1657
3. Johnson RT, Richardson EP. The neurological manifestations of systemic lupus erythematosus. Medicine (Baltimore) 1968;47:337–369
4. McCune WJ, Golbus J. Neuropsychiatric lupus. Rheum Dis Clin North Am 1988;14:149–167
5. Tola MR, Granieri E, Caniatti L, et al. Systemic lupus erythematosus presenting with neurological disorders. J Neurol 1992;239:61–64
6. Omdal R, Selseth B, Klow NE, et al. Clinical neurological, electrophysiological, and cerebral CT scan findings in systemic lupus erythematosus. Scand J Rheumatol 1989;18:283–289
7. Ellis SG, Verity MA. Central nervous system involvement in systemic lupus erythematosus: a review of neuropathologic findings in 57 cases, 1955–1977. Semin Arthritis Rheum 1979;8:212–221
8. van Dam AP. Diagnosis and pathogenesis of CNS lupus. Rheumatol Int 1991;11:1–11
9. Denburg JA, Behmann SA. Lymphocyte and neuronal antigens in neuropsychiatric lupus: presence of an elutable, immunoprecipitable lymphocyte/neuronal 52 kd reactivity. Ann Rheum Dis 1994;53:304–308
10. Devinsky O, Petitio CK, Alonso DR. Clinical and neuropathological findings in systemic lupus erythematosus: the role of vasculitis, heart emboli and thrombotic thrombocytopenia purpura. Ann Neurol 1988; 23:380–384
11. Hanly JG, Walsh NM, Sangalang V. Brain pathology in systemic lupus erythematosus. J Rheumatol 1992;19:732–741
12. Waterloo K, Omdal R, Sjoholm H, et al. Neuropsychological dysfunction in systemic lupus erythematosus is not associated with changes in cerebral blood flow. J Neurol 2001;248:595–602
13. Chinn RJ, Wilkinson ID, Hall-Craggs MA, et al. Magnetic resonance imaging of the brain and cerebral proton spectroscopy in patients with systemic lupus erythematosus. Arthritis Rheum 1997;40:36–46
14. Coban O, Bahar S, Akman-Demir G, et al. A controlled study of reliability and validity of MRI findings in neuro-Behcet's disease. Neuroradiology 1996;38:312–316
15. Gerber S, Biondi A, Dormont D, et al. Long-term MR follow-up of cerebral lesions in neuro-Behcet's disease. Neuroradiology 1996;38:761–768
16. Guma A, Aguilera C, Acebes J, et al. Meningeal involvement in Behcet's disease: MRI. Neuroradiology 1998;40:512–515
17. Hachulla E, Michon-Pasturel U, Leys D, et al. Cerebral magnetic resonance imaging in patients with or without antiphospholipid antibodies. Lupus 1998;7:124–131
18. Kozora E, West SG, Kotzin BL, et al. Magnetic resonance imaging abnormalities and cognitive deficits in systemic lupus erythematosus patients without overt central nervous system disease. Arthritis Rheum 1998;41:41–47
19. Miller DH, Ormerod IE, Gibson A, et al. MR brain scanning in patients with vasculitis: differentiation from multiple sclerosis. Neuroradiology 1987;29:226–231
20. Rovaris M, Inglese M, Viti B, et al. The contribution of fast-FLAIR MRI for lesion detection in the brain of patients with systemic autoimmune diseases. J Neurol 2000;247:29–33
21. Wynne PJ, Younger DS, Khandji A, et al. Radiographic features of central nervous system vasculitis. Neurol Clin 1997;15:779–804
22. Emmi L, Bramati M, De Cristofaro MT, et al. MRI and SPECT investigations of the CNS in SLE patients. Clin Exp Rheumatol 1993;11:13–20
23. Kodama K, Okada S, Hino T, et al. Single photon emission computed tomography in systemic lupus erythematosus with psychiatric symptoms. J Neurol Neurosurg Psychiatry 1995;58:307–311
24. Postiglione A, De Chiara S, Soricelli A, et al. Alterations of cerebral blood flow and antiphospholipid antibodies in patients with systemic lupus erythematosus. Int J Clin Lab Res 1998;28:34–38
25. Rubbert A, Marienhagen J, Pirner K, et al. Single-photon-emission computed tomography analysis of cerebral blood flow in the evaluation of central nervous system involvement in patients with systemic lupus erythematosus. Arthritis Rheum 1993;36:1253–1262
26. Chen JJ, Yen RF, Kao A, et al. Abnormal regional cerebral blood flow found by technetium-99m ethyl cysteinate dimer brain single photon emission computed tomography in systemic lupus erythematosus patients with normal brain MRI findings. Clin Rheumatol 2002;21: 516–519
27. Huang WS, Chiu PY, Tsai CH, et al. Objective evidence of abnormal regional cerebral blood flow in patients with systemic lupus erythematosus on Tc-99m ECD brain SPECT. Rheumatol Int 2002;22:178–181
28. Kao CH, Ho YJ, Lan JL, et al. Discrepancy between regional cerebral blood flow and glucose metabolism of the brain in systemic lupus erythematosus patients with normal brain magnetic resonance imaging findings. Arthritis Rheum 1999;42:61–68
29. Kao CH, Lan JL, ChangLai SP, et al. The role of FDG-PET, HMPAO-SPET and MRI in the detection of brain involvement in patients with systemic lupus erythematosus. Eur J Nucl Med 1999;26:129–134
30. Lin WY, Wang SJ, Yen TC, et al. Technetium-99m-HMPAO brain SPECT in systemic lupus erythematosus with CNS involvement. J Nucl Med 1997;38:1112–1115
31. Hossain AK, Murata Y, Zhang L, et al. Brain perfusion SPECT in patients with corticobasal degeneration: analysis using statistical parametric mapping. Mov Disord 2003;18:697–703
32. Colamussi P, Giganti M, Cittanti C, et al. Brain single-photon emission tomography with 99mTc-HMPAO in neuropsychiatric systemic lupus erythematosus: relations with EEG and MRI findings and clinical manifestations. Eur J Nucl Med 1995;22:17–24
33. Falcini F, De Cristofaro MT, Ermini M, et al. Regional cerebral blood flow in juvenile systemic lupus erythematosus: a prospective SPECT study: single photon emission computed tomography. J Rheumatol 1998;25:583–588
34. Kovacs JA, Urowitz MB, Gladman DD, et al. The use of single photon emission computerized tomography in neuropsychiatric SLE: a pilot study. J Rheumatol 1995;22:1247–1253
35. Nossent JC, Hovestadt A, Schonfeld DH, et al. Single-photon-emission computed tomography of the brain in the evaluation of cerebral lupus. Arthritis Rheum 1991;34:1397–1403
36. Russo R, Gilday D, Laxer RM, et al. Single photon emission computed tomography scanning in childhood systemic lupus erythematosus. J Rheumatol 1998;25:576–582
37. Kushner MJ, Tobin M, Fazekas F, et al. Cerebral blood flow variations in CNS lupus. Neurology 1990;40:99–102
38. Sabbadini MG, Manfredi AA, Bozzolo E, et al. Central nervous system involvement in systemic lupus erythematosus patients without overt neuropsychiatric manifestations. Lupus 1999;8:11–19
39. Tan EM, Cohen AS, Fries JF, et al. The 1982 revised criteria for classification of systemic lupus erythematosus. Arthritis Rheum 1982;25: 1271–1277
40. World Health Organization. The ICD-10 Classification of Mental and Behavioural Disorders: Diagnostic Criteria for Research. Geneva, Switzerland: World Health Organization; 1993
41. Carbotte RM, Denburg SD, Denburg JA. Cognitive dysfunction and

systemic lupus erythematosus. In: Lahita RG, ed. Systemic Lupus Erythematosus. New York, NY: Churchill Livingstone; 1992:865–881
42. Denburg JA, Carbotte RM, Denburg SD. Neuronal antibodies and cognitive dysfunction in systemic lupus erythematosus. Neurology 1987;37:464–467
43. Gladman D, Ginzler E, Goldsmith C, et al. The development and initial validation of the Systemic Lupus International Collaborating Clinics/American College of Rheumatology damage index for systemic lupus erythematosus. Arthritis Rheum 1996;39:363–369
44. Folstein MF, Folstein SE, McHugh PR. "Mini-Mental State": a practical method for grading the cognitive state for the clinician. J Psychiatr Res 1975;12:189–198
45. O'Tuama LA, Treves ST. Brain single-photon emission computed tomography for behavior disorders in children. Semin Nucl Med 1993; 23:255–264
46. Friston KJ, Holmes AP, Worsley KJ, et al. Statistical parametric maps in functional imaging: a general linear approach. Hum Brain Mapp 1995;2:189–210
47. Friston KJ, Holmes AP, Poline JB, et al. Detecting activations in PET and fMRI: levels of inference and power. Neuroimage 1996;40:223–235
48. Talairach J, Tournoux P. Co-planar Stereotaxic Atlas of the Human Brain. Three-Dimensional Proportional System: An Approach to Cerebral Imaging. New York, NY: Thieme Medical Publishers; 1988
49. Ashburner J, Neelin P, Collins DL, et al. Incorporating prior knowledge into image registration. Neuroimage 1997;6:344–352
50. Zvaifler NJ, Bluestein HG. The pathogenesis of central nervous system manifestations of systemic lupus erythematosus. Arthritis Rheum 1982; 25:862–866
51. Belmont HM, Abramson SB, Lie JT. Pathology and pathogenesis of vascular injury in systemic lupus erythematosus: interactions of inflammatory cells and activated endothelium. Arthritis Rheum 1996;39:9–22
52. Grunwald F, Schomburg A, Badali A, et al. 18FDG PET and acetazolamide-enhanced 99m Tc-HMPAO SPET in systemic lupus erythematosus. Eur J Nucl Med 1995;22:1073–1077
53. Szer IS, Miller JH, Rawlings D, et al. Cerebral perfusion abnormalities in children with central nervous system manifestations of lupus detected by single photon emission computed tomography. J Rheumatol 1993;20: 2143–2148
54. Desgranges B, Baron JC, de la Sayette V, et al. The neural substrates of memory systems impairment in Alzheimer's disease: a PET study of resting brain glucose utilization. Brain 1998;121:611–631
55. Minoshima S, Foster NL, Kuhl DE. Posterior cingulate cortex in Alzheimer's disease [letter]. Lancet 1994;344:895
56. Minoshima S, Giordani B, Berent S, et al. Metabolic reduction in the posterior cingulate cortex in very early Alzheimer's disease. Ann Neurol 1997;42:85–94
57. Matsuda H, Kitayama N, Ohnishi T, et al. Longitudinal evaluation of both morphologic and functional changes in the same individuals with Alzheimer's disease. J Nucl Med 2002;43:304–311
58. Vogt BA, Finch DM, Olson CR. Functional heterogeneity in cingulate cortex: the anterior executive and posterior evaluative regions. Cereb Cortex 1992;2:435–443
59. Drevets WC, Raichle ME. Neuroanatomical circuits in depression: implications for treatment mechanisms. Psychopharmacol Bull 1992; 28:261–274
60. Kapur S, Meyer J, Wilson AA, et al. Modulation of cortical neuronal activity by a serotonergic agent: a PET study in humans. Brain Res 1994;646:292–294
61. Smith DF, Geday J. PET neuroimaging of clomipramine challenge in humans: focus on the thalamus [Erratum in Brain Res 2001;903:269]. Brain Res 2001;892:193–197
62. Byne W, Buchsbaum MS, Mattiace LA, et al. Postmortem assessment of thalamic nuclear volumes in subjects with schizophrenia. Am J Psychiatry 2002;159:59–65
63. Pakkenberg B. Pronounced reduction of total neuron number in mediodorsal thalamic nucleus and nucleus accumbens in schizophrenics. Arch Gen Psychiatry 1990;47:1023–1028
64. Popken GJ, Bunney WE Jr, Potkin SG, et al. Subnucleus-specific loss of neurons in medial thalamus of schizophrenics. Proc Natl Acad Sci U S A 2000;97:9276–9280
65. Young KA, Manaye KF, Liang C, et al. Reduced number of mediodorsal and anterior thalamic neurons in schizophrenia. Biol Psychiatry 2000; 47:944–953
66. Vasile RG, Sachs G, Anderson JL, et al. Changes in regional cerebral blood flow following light treatment for seasonal affective disorder: responders versus nonresponders. Biol Psychiatry 1997;42:1000–1005
67. Oda K, Okubo Y, Ishida R, et al. Regional cerebral blood flow in depressed patients with white matter magnetic resonance hyperintensity. Biol Psychiatry 2003;53:150–156
68. Awada HH, Mamo HL, Luft AG, et al. Cerebral blood flow in systemic lupus erythematosus with and without central nervous system involvement. J Neurol Neurosurg Psychiatry 1987;50:1597–1601
69. Miller DD, Andreasen NC, O'Leary DS, et al. Comparison of the effects of risperidone and haloperidol on regional cerebral blood flow in schizophrenia. Biol Psychiatry 2001;49:704–715
70. Nobler MS, Roose SP, Prohovnik I, et al. Regional cerebral blood flow in mood disorders, 5: effects of antidepressant medication in late-life depression. Am J Geriatr Psychiatry 2000;8:289–296

Psychopharmacology (2006) 185: 395–399
DOI 10.1007/s00213-005-0304-0

ORIGINAL INVESTIGATION

Akihiro Takano · Kazutoshi Suzuki · Jun Kosaka · Miho Ota · Shoko Nozaki · Yoko Ikoma · Shuji Tanada · Tetsuya Suhara

A dose-finding study of duloxetine based on serotonin transporter occupancy

Received: 21 November 2005 / Accepted: 19 December 2005 / Published online: 28 February 2006

Abstract *Rationale:* Positron emission tomography (PET) has been utilized for determining the dosage of antipsychotic drugs. To evaluate the dosage of antidepressants such as selective serotonin reuptake inhibitors, serotonin transporter occupancy (5-HTT) is also a useful index. *Objectives:* We investigated the degree of 5-HTT occupancy with different doses of the antidepressant duloxetine and the time-course of 5-HTT occupancy using PET. *Methods:* PET scans with [^{11}C]DASB were performed before and after a single administration of duloxetine (5–60 mg), and three consecutive scans were performed after a single dose or repeated doses of 60 mg of duloxetine. *Results:* 5-HTT occupancies by duloxetine were increased by 35.3 to 86.5% with dose and plasma concentration increments. The ED_{50} value of 5-HTT occupancy was 7.9 mg for dose and 3.7 ng/ml for plasma concentration. In the time-course of 5-HTT occupancy, mean occupancies were 81.8% at 6 h, 71.9% at 25 h, and 44.9% at 53 h after a single administration, and 84.3% at 6 h, 71.9% at 49 h, and 47.1% at 78 h after repeated administrations. *Conclusions:* Based on 5-HTT occupancy, 40 mg and more of duloxetine was needed to attain 80% occupancy, and 60 mg of duloxetine could maintain a high level of 5-HTT occupancy with a once-a-day administration schedule.

A. Takano · K. Suzuki · J. Kosaka · M. Ota · S. Nozaki · Y. Ikoma · T. Suhara (✉)
Molecular Imaging Center,
National Institute of Radiological Sciences,
9-1, Anagawa 4-Chome, Inage-ku,
Chiba, 263-8555, Japan
e-mail: suhara@nirs.go.jp
Tel.: +81-43-2063194
Fax: +81-43-2530396

S. Tanada
Department of Medical Imaging,
National Institute of Radiological Sciences,
9-1, Anagawa 4-Chome, Inage-ku,
Chiba, 263-8555, Japan

Keywords Duloxetine · Occupancy · 5-HTT · PET · DASB · Time-course

Introduction

Positron emission tomography (PET) studies have made it possible to investigate the in vivo neurotransmission in the living human brain (Farde et al. 1988). Investigations for optimizing the dosage of various CNS drugs based on the relationship between in vivo occupancy and dose/plasma concentration have been reported (Mamo et al. 2004; Andree et al. 2003). The advantage of in vivo receptor occupancy studies using PET was realized from the fact that it revealed inappropriate clinical dose settings of old antipsychotics (Takano et al. 2006). Radio-labeled ligands such as [^{11}C]McN(+)5652 and [^{11}C]DASB have been used to visualize and quantify serotonin transporter (5-HTT) in the brain, and [^{11}C]DASB has relatively higher binding potentials for 5-HTT (Wilson et al. 2000b). Recently, high 5-HTT occupancy by selective serotonin reuptake inhibitors (SSRIs) during the treatment of mood disorder has been reported (Meyer et al. 2001, 2004; Suhara et al. 2003). 5-HTT occupancy was reported to be over 80% at clinical doses of antidepressants such as SSRIs and tricyclic ones during the treatment of depression (Meyer et al. 2001, 2004; Suhara et al. 2003). It was also suggested that investigation of the time-course of receptor occupancy by CNS drugs would help to determine the administration schedule (Tauscher et al. 2002; Takano and Suhara 2005).

Duloxetine is one of the serotonin noradrenaline reuptake inhibitors (Wong 1998), and several double-blind, placebo-controlled clinical trials have demonstrated its efficacy for major depressive disorder (Goldstein et al. 2002; Detke et al. 2004, 2002a,b; Brannan et al. 2005a,b). However, the relationship between dose/plasma concentration and occupancy of the binding site in the brain and the kinetics at the binding site of duloxetine has not been fully explored.

In this study, we investigated the degree of 5-HTT occupancy by different doses of duloxetine and the time-course of 5-HTT occupancy using PET.

Materials and methods

Seventeen healthy male volunteers were enrolled in this study. None had a history of present or past psychiatric, neurological, or somatic disorders, and they had no alcohol- or drug-related problems. They had not taken any kind of medication for at least 1 month before the start of the study. All were nonsmokers. Two volunteers were excluded for PET-related technical reasons. Therefore, 15 healthy male volunteers (24.1+2.4 years old) completed the study. The study was approved by the ethics and radiation safety committees of the National Institute of Radiological Sciences, Chiba, Japan. Written informed consent was obtained from each subject.

Radioligand

[^{11}C]DASB was synthesized by methylation of the corresponding des-methyl precursor with [^{11}C]CH_3I (Wilson et al. 2000a,b). Radiochemical purities were over 95%.

PET studies

The PET study consisted of the two following parts.

Part A: single administration study

Of 15 subjects, 12 subjects participated in the Part A study. Three volunteers each took a single oral dose of 5, 20, 40, or 60 mg of duloxetine. The first PET scan was performed before the duloxetine administration as a baseline study. The second PET scan was performed 6 h after the single-dose administration. A third scan was performed 25 h after administration on the three volunteers taking 60 mg, and this was followed by a fourth scan at 53 h.

Part B: repeated administration study

Three volunteers took 60 mg of duloxetine daily for 7 days. The first PET scan was performed before the duloxetine administration as a baseline study. The second PET scan was performed 6 h after the last administration. Additional scans were performed at 49 and at 78 h after the last administration.

PET procedures

PET scans were carried out with a ECAT 47 (CTI-Siemens, Knoxville, TN, USA) scanner. A head fixation device was used during the scans (Fixter Instruments, Stockholm, Sweden). A 10-min transmission scan was done to correct for attenuation. Dynamic PET scans were carried out for 90 min (1 min×4, 2 min×13, 4 min×5, 8 min×5) in 2-D mode immediately after a bolus injection of 603.8–855.1 (mean±SD, 728.3±47.7) MBq of [^{11}C]DASB with high specific radioactivities (41.1–168.6 GBq/μmol; mean±SD, 98.3±31.5 GBq/μmol).

MRI procedures

T1-weighted images of the brain were obtained by Gyroscan NT (Phillips Medical Systems, Best, The Netherlands) (1.5T).

Plasma concentration of duloxetine

Blood samples were taken to measure the concentrations of duloxetine just before and after each PET scan. The plasma concentrations of duloxetine were determined by LC-MS/MS (Prevalere Life Sciences, NY, USA).

Data analysis

All emission scans were reconstructed with a Ramp filter cutoff frequency of 0.5. The data were not subjected to motion correction. Regions of interest for the thalamus and cerebellum were drawn on the coregistered PET/MRI images using a template-based method (Yasuno et al. 2002).

Quantification was performed using multilinear reference tissue model 2 (Ichise et al. 2003), which was originally developed based on [^{11}C]DASB data. The cerebellum was used as the reference tissue because of its negligible density of 5-HTT. These models allow the estimation of binding potential (BP), which was defined as the ratio of receptor density (B_{max}) to dissociation constant (K_d).

The 5-HTT occupancy was calculated by the following equation:

$$\text{Occu} = \left(\text{BP}_{\text{baseline}} - \text{BP}_{\text{drug}}\right) \times 100/\text{BP}_{\text{baseline}},$$

where Occu is the 5-HTT occupancy, $\text{BP}_{\text{baseline}}$ is BP in the drug-free state, and BP_{drug} is BP of the subjects with the drug.

The relationship between plasma concentration and 5-HTT occupancy was modeled by the following equation: $\%5\text{-HTT occupancy} = 100 \times C/(\text{ED}_{50} + C)$, where %5-HTT occupancy is the percentage of 5-HTT occupied, ED_{50} is a constant, and C is the concentration of the drug in the vicinity of transporters; dose and plasma concentration of duloxetine just before each PET scan were used as functional surrogates of C.